JNeurosci
THE JOURNAL OF NEUROSCIENCE

Research Articles: Development/Plasticity/Repair

Maturation of Brain Microstructure and Metabolism Associates with Increased Capacity for Self-Regulation during the Transition from Childhood to Adolescence

https://doi.org/10.1523/JNEUROSCI.2422-18.2019

Cite as: J. Neurosci 2019; 10.1523/JNEUROSCI.2422-18.2019

Received: 19 September 2018
Revised: 30 July 2019
Accepted: 5 August 2019

Maturation of Brain Microstructure and Metabolism Associates with Increased Capacity for Self-Regulation during the Transition from Childhood to Adolescence

Running title: Brain maturation and improving cognitive capacities

Mary Baron Nelson PhD[1,2], Sharon H. O'Neil PhD[1,3,4], Jessica L. Wisnowski PhD[1,5,9], Danielle Hart BS[6], Siddhant Sawardekar MS[6], Virginia Rauh ScD[8,10], Frederica Perera DrPH PhD[8,11], Howard F. Andrews PhD MS[13], Lori A. Hoepner DrPH[11,12], Wanda Garcia[8,10], Molly Algermissen PhD[14], Ravi Bansal PhD[1,5], Bradley S. Peterson MD[1,4,6,7]

[1]Department of Pediatrics, Keck School of Medicine at USC, Los Angeles, CA 90027
[2]Division of Cancer & Blood Diseases, Children's Hospital Los Angeles, CA 90027
[3] Division of Neurology, Children's Hospital Los Angeles, CA 90027
[4]The Saban Research Institute, Children's Hospital Los Angeles, CA 90027
[5]Department of Radiology, Children's Hospital Los Angeles, CA 90027
[6]Institute for the Developing Mind, Children's Hospital Los Angeles, CA 90027
[7]Department of Psychiatry, Keck School of Medicine at University of Southern California, Los Angeles, CA 90027
[8]Columbia Center for Children's Environmental Health, New York, New York 10025
[9]Division of Neonatology, Children's Hospital Los Angeles
[10]Department of Population and Family Health, Mailman School of Public Health, Columbia University, New York, New York 10025
[11]Department of Environmental Health Sciences, Mailman School of Public Health, Columbia University, New York, New York 10025
[12]Department of Environmental and Occupational Health Sciences, SUNY Downstate School of Public Health, Brooklyn, New York 10025
[13]Biostatistics Department, Mailman School of Public Health, Columbia University, New York, New York 10025
[14]Department of Psychiatry, Columbia University, New York, New York 10025

Corresponding author: Bradley Peterson, MD Institute for the Developing Mind, Children's Hospital Los Angeles, 4650 Sunset Blvd., MS #135, CA 90027. bpeterson@chla.usc.edu

Number of pages: 28
Number of figures: 8
Number of tables: 3
Number of words, Abstract: 189
Introduction: 627
Discussion: 1499
Conflict of Interest: The authors declare no competing financial interests

Acknowledgement: This research was made possible by the provision of data by New York State Psychiatric Institute and Columbia University, and with funding from 2 P50 ES009600 (NIEHS), EPA 83615401, 1R01DA027100 (NIDA), 5R01ES015579 (NIEHS).
The authors wish to thank the Neuropsychology Core at The Saban Research Institute of Children's Hospital Los Angeles for its support.

Abstract

Children ages 9-12 years face increasing social and academic expectations that require mastery of their thoughts, emotions, and behavior. Little is known about the development of neural pathways integral to these improving capacities during the transition from childhood to adolescence. Among 234 healthy, inner-city male and female youth (species *homo sapiens*) 9-12 years of age followed by the Columbia Center for Children's Environmental Health (CCCEH), we acquired Diffusion Tensor Imaging (DTI), Multiplanar Chemical Shift Imaging (MPCSI), and cognitive measures requiring self-regulation. We found that increasing age was associated with increased fractional anisotropy (FA) and decreased apparent diffusion coefficient (ADC), most prominently in the frontal and cingulate cortices, striatum, thalamus, deep white matter, and cerebellum. Additionally, we found increasing age was associated with increased N-Acetyl-L-aspartate (NAA) in the anterior cingulate and insular cortices, and decreased NAA in posterior cingulate and parietal cortices. Age-associated changes in microstructure and neurometabolite concentrations partially mediated age-related improvements in performance on executive function tests. Taken together, these findings suggest that maturation of key regions within cortico-striatal-thalamo-cortical (CSTC) circuits subserve the emergence of improved self-regulatory capacities during the transition from childhood to adolescence.

64 **Significance Statement**

65 Few imaging studies of normal brain development have focused on a population of inner-city,
66 racial/ethnic minority youth during the transition from childhood to adolescence, a period when
67 self-regulatory capacities rapidly improve. We used DTI and MPCSI to provide unique windows
68 into brain maturation during this developmental epoch, assessing its mediating influences on
69 age-related improvement in performance on self-regulatory tasks. Our findings suggest that
70 rapid maturation of cortico-striato-thalamo-cortical (CSTC) circuits, represented as progressive
71 white matter maturation (increasing FA and increasing NAA, Ch, Cr concentrations
72 accompanying advancing age) in frontal regions and related subcortical projections and
73 synaptic pruning (decreasing NAA, Ch, Cr, Glx) in posterior regions, support age-related
74 improvements in executive functioning and self-regulatory capacities in youth 9-12 years of age.
75

Introduction

The transition from childhood to adolescence is a time of emergence and strengthening of the ability to regulate thought, emotion, and behavior in the context of increasing societal demands on intellectual ability, academic performance, and interpersonal relationships. Self-regulation -- monitoring and controlling one's own thoughts, emotions and actions -- supports flexible, goal-directed behavior. It is critical to academic and social competence (Nigg, 2016), and to maintaining emotional health. The neural circuits that support self-regulation include gray matter of the frontal cortex, basal ganglia, and thalamus, gray matter structures interconnected via white matter axonal pathways projecting through the centrum semiovale, corona radiata, and internal capsule. These frontostriatal circuits are a component of the larger cortico-striato-thalamo-cortical loops (CSTC) (Marsh et al., 2009a) that include dorsolateral prefrontal cortex (DLPFC), anterior cingulate cortex, supplementary motor area, ventral and lateral orbitofrontal cortex, and temporal cortices, all of which have connections with the basal ganglia and thalamus (Peterson et al., 1999; Leung et al., 2000; Peterson et al., 2002). The dorsal portions of these circuits subserve neuropsychological tasks requiring response inhibition, or the ability to supersede prepotent responses with responses designated instead by task instructions, which is a form of self-regulation (Peterson et al., 2003; Marsh et al., 2009a). Response inhibition strengthens during late childhood and adolescence and is thought to depend on the dorsolateral and ventrolateral prefrontal cortices and their connections to the basal ganglia (Dubin et al., 2010).

Despite abundant evidence that dysfunction in these circuits underlies a wide range of developmental psychopathologies, including attention-deficit/hyperactivity disorder (Pavuluri et al., 2009; Rubia, 2011), tic disorders (Marsh et al., 2007), obsessive-compulsive disorder (Goncalves et al., 2016), addictions (Volkow et al., 2016), and eating disorders (Marsh et al., 2009b; Jauregui-Lobera, 2016; Kessler et al., 2016), relatively little is known about the cellular

and microstructural changes in these circuits that support the maturation of self-regulatory skills in the transition from childhood to adolescence.

The aim of this study was to identify the age correlates of cerebral microstructure and neurometabolite concentrations in a large cohort of typically developing, racial and ethnic minority youth, 9-12 years of age. This is the time in development when children enter middle school and mobilize self-regulatory capacities to meet rapidly increasing academic and social demands. We also aimed to assess whether these brain measures mediate the association of advancing age with better performance on cognitive tasks requiring self-regulation.

We elected to use Diffusion Tensor Imaging **(DTI)** and Multi-Planar Chemical Shift Imaging (**MPCSI**) to measure brain maturation in CSTC pathways. DTI characterizes the three-dimensional diffusion of water as a function of spatial location, providing information about developing white matter organization, integrity, and myelination. MPCSI, a relatively recent advance in MR spectroscopy (MRS) methodology, provides a metabolic map of brain metabolites in 1 cc voxels throughout the brain, with a degree of spatial resolution not possible using more conventional, single-voxel MRS. Combining these two modalities permits a deeper exploration of brain tissue organization and cellular characterization of CTSC pathways in the late grade school-age child. Self-regulation was assessed using measures of performance on standardized psychometric tasks requiring attention, response inhibition, and cognitive flexibility. Additionally, we assessed visual-motor integration, as it requires similarly complex circuits to integrate visual, motor, and planning components of the task. We conducted *post hoc* mediation analyses to test whether brain measures mediated age-related improvement in psychometric performance.

Our *a priori* hypotheses were that (1) age would correlate significantly with measures of cerebral microstructure (FA, ADC) and neurometabolite concentrations (NAA) in CTSC pathways, representing progressive brain maturation from ages 9 to 12; and (2) FA and NAA measures within CTSC pathways would mediate the age-related improvement in performance

on executive function tests, indicating that maturation of CTSC pathways support an increasing capacity for self-regulation during this period of development.

Materials and Methods

Experimental Design This was a cross-sectional neuroimaging and psychometric study of children ages 9-12 years who underwent assessment as part of a larger prospective, longitudinal study described below.

Sampling Frame This study population of 9 to12 year-old youth was selected from a birth cohort of the Columbia Center for Children's Environmental Health (CCCEH). The cohort comprised 727 children born to urban, non-smoking mothers 18-35 years of age who were without diabetes, hypertension, and HIV. Pregnant women were recruited from 1998-2006 through prenatal clinics as part of a prospective, longitudinal study of environmental exposures in a representative sample of low-income, African-American and Latino women in northern Manhattan. By 2014, 204 participants had withdrawn from the study or had not been recently assessed, leaving 523 participants. The demographics (age, sex, race/ethnicity, maternal age or education) of children who discontinued participation did not differ significantly from those who continued in the study. From this sample of 523 participants, we were able to obtain MRI scans in 309 of the children, 5 to 14 years of age. Our primary analyses focused on the 280 children who were 9-12 years of age, a time when intellectual and self-regulatory capacities develop rapidly. Restricting the age range to 9-12 years also provided a much more uniform age distribution in the sample (Fig.1), supporting more robust statistical analyses and inferences about the age-related effects of brain maturation during the transition from childhood to adolescence. In addition, we conducted *post hoc* tests across the entire cohort from 5-14 years of age to determine whether the age correlations in brain microstructure and metabolite concentrations generalized to the wider age range from childhood to adolescence.

[Figure 1]

Of the 319 participants in the more restricted age range, 280 had imaging data obtained within 10 days of psychometric assessment; 168 children had both DTI and MPCSI data, 66 had usable DTI but no MPCSI data, and 46 had MPCSI data but no usable DTI data. Thus, the final DTI sample was 234 (66+168) and consisted of 128 females and 106 males, and the MPCSI sample was 218 (46+168), consisting of 116 females and 102 males. Fewer children had spectroscopy data, as MPCSI was the last sequence of the scanning protocol; thus, if children were unable to complete the entire scan, spectroscopy was not obtained. Additionally, 29 participants aged 5-8 and 13-14 had imaging and psychometric data available for post hoc analyses.

Participant Characterization and Study Procedures We obtained written informed consent from parents and assent from children. The study was approved by the Institutional Review Boards at the New York State Psychiatric Institute and Columbia University. Participants were paid for their participation.

Participants completed approximately 3-hours of neuropsychological assessment with standardized psychometric measures evaluating intellectual functioning, attention, working memory, processing speed, executive functions, fine motor dexterity, and visual-motor integration in a controlled testing environment. Breaks were provided to minimize fatigue. Mothers completed questionnaires about demographics, education, home environment and material hardship, and standardized surveys of their children's social, emotional, and behavioral functioning. The assessment was performed in a single session.

Neuropsychological tests were administered by research assistants trained on the administration and scoring of each measure by a pediatric neuropsychologist. From the extensive neuropsychological constructs assessed in the larger study, we selected raw scores of the following measures for correlation analyses, as they were most relevant to testing our *a priori* hypotheses of brain-based mediation of age-related improvements in cognitive performance in the peripubertal period: (1) The *Conners' Continuous Performance Test, Second*

178 *Edition* (**CPT-II**) (Conners, 1994). This is a 15-minute computerized test of basic sustained
179 attention, attentional capacity and inhibitory control. The CPT-II provides individual performance
180 scores for a range of cognitive processes including inattention (omission errors), inhibition and
181 impulsivity (commission errors), reaction time, and the ability to discriminate targets from non-
182 targets (d'). (2) The *Developmental Neuropsychological Assessment, Second Edition* (**NEPSY-**
183 **II**) (Kemp et al., 2007). This is a standardized battery of tests of executive functions, language,
184 learning, sensorimotor functions, visuospatial processing and social perception. From this
185 battery, we selected the Auditory Attention, Response Set, Inhibition, Inhibition/Switching, and
186 Design Copying subtests. These measures assess selective and sustained auditory attention,
187 response inhibition, cognitive flexibility, and visuospatial processing, respectively.
188 **Imaging Measures** DTI indices included fractional anisotropy (FA) and apparent diffusion
189 coefficient (ADC). FA is a measure of directionally dependent diffusion, where higher values
190 reflect increased structural integrity and degree of alignment within white matter fiber tracts
191 (Cercignani et al., 2001; Mukherjee et al., 2002). ADC measures diffusion independent of
192 direction. Radial and axial diffusivity (RD, AD) are two additional directional measures, with RD
193 indicating diffusion rate perpendicular to the principal direction of diffusion, and AD indicating
194 diffusion rate along the same direction as the principal (Feldman et al, 2010).
195 MPCSI quantifies brain metabolites to assess cellular function and metabolism (Goh et
196 al, 2014). NAA is a putative index of the density of viable neurons, Ch is a marker of membrane
197 turnover and may reflect alterations in cell density, Cr is a marker of metabolic activity (Rae,
198 2014), and Glx is an index of energy metabolism and neurotransmission (Ramadan et al.,
199 2013).
200 **MRI Data Acquisition** DTI and MPCSI data were acquired using a 3.0T Signa MR Scanner
201 (GE Healthcare, Milwaukee, WI) equipped with an 8-channel receive head coil. Extra time was
202 allowed on the morning of the scan to acclimate the participant to the MRI and its noise.
203 Anxious children were calmed with frequent reminders, praise, and relaxation techniques,

allowing for acquisition of motion-free data. During the scan, high quality images were assured in real time with strict oversight of the data appearing on the console. If motion artifact was detected, sequences were repeated either the same day or the next day. Pulse sequences included the following:

Anatomical MRI High-resolution T1-weighted **(T1w)** anatomical images were acquired with a 3D Fast Spoiled Gradient Recall (FSPGR) sequence with sagittal reconstruction: repetition time (TR)=2170 msec, echo time (TE)=1.3 msec, inversion time=500 msec, flip angle=11°, matrix=256x256, field of view=25 cm, phase field of view=100%, slice thickness=1.0 mm, acceleration factor=2, number of slices=160, voxel size=1x1x1mm^3. Two images each of NEX=1 were acquired and then averaged offline.

Diffusion Tensor Imaging **(DTI)** DTI data were acquired in oblique slices parallel to the AC-PC line using single-shot echo-planar imaging sequences with matrix=132x128 zero-padded to 256x256, TR=8000 ms, TE= ~74 ms, FOV=24 cm, Flip=90^0, Slices=60, Slice thickness=2.5 mm, Slice Spacing=0 mm; NEX=2, PFOV=1.0. Three baseline images were acquired with b=0 s/mm^2 and 15 diffusion weighted images **(DWIs)** with b=1000 s/mm^2 along directions that sampled the space uniformly. Phase correction and ASSET acceleration factor of 2 were applied.

Multiplanar Chemical Shift Imaging **(MPCSI)** data were acquired in 6 axial oblique slices parallel to the AC-PC line, with the second bottom-most slice containing the AC-PC plane. Pulse sequence parameters included TE=144 ms, TR=2800 ms, field of view=24 cm, slice thickness=10.0 mm, slice spacing=2.0, number of phase encoding steps=24x24, NEX=1, spectral width=2000 Hz, number of complex data points=512. Water signal was suppressed using the CHESS sequence and lipid signal from outside the brain was suppressed with 8 angulated saturation bands around the brain. MPCSI data were spatially registered to a template brain using a localizer image of high in-plane resolution in the same orientation and slice locations as the MPCSI data. Those images were acquired with TR=300 ms, TE=10 ms,

FOV=24 cm, slice thickness=10.0 mm, spacing=2.0 mm, acquisition matrix=256x128, image zero-padded to 256x256.

Anatomical MRI Segmentation The high resolution T1-weighted anatomical images were segmented into gray and white matter for use in partial volume correction of MPCSI data. Brain was isolated from non-brain tissue using an automated brain extraction tool (BrainSuite, RRID:SCR_006623) (Shattuck and Leahy, 2002) followed by manual editing using an inhouse generated program to remove any dura that remained connected to the brain. Next, a thresholding technique based on a representative sampling of gray and white matter values was used to segment brain tissue as gray or white matter. These anatomical images were then registered across participants in template space. Segmentation and registration were completed using inhouse codes described elsewhere (Colibazzi et al., 2008).

DTI Processing. We conducted quality assurance procedures to exclude datasets with excessive motion. This included quantifying head motion for each participant using 2 summary statistics, the Root Mean Squared (RMS) (Jenkinson et al., 2002) and Mean Frame-wise Displacement (FD) metrics, both of which sum differentiated realignment estimates (Power et al., 2012) derived from 3 translational (x,y,z) and 3 angular rotation (roll, pitch, yaw) variables. Images with >0.5 mm motion were removed from further preprocessing; if >10% of images had this much motion, that dataset was excluded from further processing. Next, we used quadratic warping along the anterior-posterior direction to correct for spatial distortions induced by eddy currents in the phase-encoding direction (Haselgrove and Moore, 1996). We also assessed motion by constructing tensor color maps from the retained images and visually assessing the principal eigenvectors throughout the brain, which show a color bias in the presence of motion artifact.

From the pre-processed data, we computed the measures for a priori hypothesis testing, FA and ADC, as well as secondary measures, axial diffusivity (AD) and radial diffusivity (RD), voxel-wise across the brain (DSI Studio, RRID:SCR_009557). A diffusion tensor D was fit to the

DWI data to ensure positive definiteness of the fitted tensor by first decomposing the tensor D as the product D = A*A^T to estimate matrix A, and then using the estimated matrix $\tilde{A}$ to compute the positive definite tensor $\tilde{D} = \tilde{A} * \tilde{A}^T$. The positive definite tensor was decomposed into its eigenvalues $(\lambda_1, \lambda_2, \lambda_3)$ and eigenvectors (v_1, v_2, v_3), which were then used to compute $FA = \frac{\sqrt{(\lambda_1-\lambda_2)^2+(\lambda_2-\lambda_3)^2+(\lambda_3-\lambda_1)^2}}{\sqrt{2*(\lambda_1^2+\lambda_2^2+\lambda_3^2)}}$, $ADC = \frac{1}{3}(\lambda_1 + \lambda_2 + \lambda_3)$, $AD = \lambda_1$. and $RD = \frac{1}{2}(\lambda_2 + \lambda_3)$.

FA, our primary measure, depicts the degree of directionality of water diffusion and is thought to represent the degree of local organization of white matter fibers and integrity of tissue microstructure (Alexander et al., 2007). ADC, also a primary measure, represents the magnitude of water diffusion, while AD and RD describe respectively the magnitude of diffusion parallel and perpendicular to the primary axis of the diffusion tensor. When considered together, maps of FA, ADC, RD, and AD aid interpretation of the biological basis for DTI findings.

Spatial Normalization of DTI Data DTI data and its derived measures from all participants were spatially coregistered into the coordinate space of a template brain. This template was an artifact-free DTI dataset from a single individual of the same age as the modal age for all participants in the cohort. Each participant brain was coregistered to the template by applying an affine transformation (3 translations, 3 rotations, and 3 scaling parameters) to the participant brain that maximized the mutual information (Viola, 1995) between the B0 images of the participant and the template brains. Then the coregistered participant's B0 image was warped to the template B0 image using a high-dimensional, nonlinear deformation based on fluid flow dynamics (Christensen et al., 1994). Finally, the same affine transformation and nonlinear deformation were applied to register the participant's FA, ADC, RD, and AD maps to the template.

MPCSI Processing MRS data quality was assured by reconstructing the data, assessing it for excess noise, and examining the spectrum in each voxel for baseline distortions, signal contamination by lipid signal from the scalp, incorrect placement of suppression bands, or

broadening of line width. Sequences containing any of these artifacts were not processed further. We processed the signal from each coil of the 8-channel head coil separately before combining their processed MRS signals to generate the spectroscopic images (Dong and Peterson, 2007). First we phase-aligned signals, then smoothed the aligned signals using a Hamming window filter, spatially reconstructed the time-domain free induction decay (FID) signal in each slice with a 2D Fourier transform, suppressed residual water signal by applying a high pass filter to the FID signal, performed line broadening using a 4 Hz Gaussian filter, and then transferred the time-domain signal into the frequency domain with a 1D Fourier transform (Hao et al., 2013). Finally, the processed frequency-domain signal from each of the 8 coils was combined by computing their weighted sum (MATLAB, RRID:SCR_01622). The combined signal was then loaded into the software *3DiCSI* (3D Interactive Chemical Shift Imaging, RRID:SCR_002581) to identify MRS voxels within the brain and save spectral data for those voxels. Spectral fitting was applied to the frequency-domain signal by identifying peaks for N-acetylaspartate (NAA), creatine (Cr), choline (Ch), glutamate + glutamine (Glx), and lipids, with a modeling spectrum for those peaks of Gaussian-Lorentzian curves. The areas under the fitted curves provided estimated concentrations of metabolites for each voxel of the brain.

Background noise for the MRS spectrum was computed as the standard deviation of the real part of the complex spectrum free from the metabolite signal. We then calculated the signal-to-noise ratio (SNR) for each metabolite concentration. The average SNR for the NAA metabolite was greater than 280 -- an excellent SNR, and attributable to use of the 8-channel head coil. A spectroscopic image (SI) for each metabolite was generated next as the ratio of the peak area to the background noise for each MRS voxel within the brain. We used the ratio of the peak area to the background noise as our dependent measure when assessing the age correlates of each metabolite concentration because it accounted for variations in receiver and transmitter gain within the MRS data across participants. Because we suppressed water signal, we were unable to calculate metabolite ratios using water as the reference. We elected to

measure each neurometabolite individually, rather than as a ratio to creatine (a common practice in spectroscopy research), for several reasons. First, ratios multiply noise in the numerator and denominator and are generally undesirable for statistical analyses. Second, ratios may lead to erroneous inferences in developmental studies because both the numerator and denominator can vary with age, in which case interpreting the age correlates of the ratio requires that the effects of the numerator and denominator be assessed separately to understand which metabolite is driving the ratio findings. Our use of metabolite concentrations normalized to noise values overcomes these difficulties and provides a much clearer understanding of the age correlates of brain metabolite levels.

The spectroscopic images were also processed to correct for both partial volume effects within each MRS voxel and the spread of MRS signal of each voxel to its neighboring voxels (i.e., the point spread function, **PSF**). The spread of MRS signal from one voxel to its neighbors derives from the use of a small number of k-space samples when acquiring the spectroscopic data and from smoothing the data with a Hamming window prior to spatial reconstruction. We estimated the PSF by simulating the acquisition of MRS data within k-space on a 24x24 grid and then spatially filtering the simulated data using a Hamming window. The resulting 24x24 complex array was interpolated to 256x256 to match the spatial resolution of the T1-weighted MR images. Partial volume effects reference the fact that an MRS voxel may contain more than one tissue type – i.e., gray matter (GM) and white matter (WM) -- in varying proportions; therefore, the signal in that voxel is a proportionate combination of signals from each of those tissues. To estimate the proportions of GM and WM within an MRS voxel, brain tissue was segmented as either GM or WM, as described above, within the participant's high-resolution ($1mm^3$ voxel) T1-weighted image, and then coregistered to the MRS data of that participant (detailed below). We then convolved the coregistered tissue definitions with the PSF function and computed the fractions of GM and WM within each MRS voxel. We next used a linear regression model (Lebon et al., 2002) at each voxel i and for each metabolite j, along with the

concentrations S_{ij} of that metabolite in the neighboring voxels, to estimate the concentration of that metabolite within gray matter M_{ij}^{G} and white matter M_{ij}^{W}:

$$S_{ij} = \left| c_i^G * M_{ij}^G + c_i^W * M_{ij}^W \right| + n$$

where c_i^G and c_i^W are the proportions of GM and WM, respectively, at voxel i and n is noise. We then tri-linearly resampled the metabolite concentrations M_{ij}^{G} and M_{ij}^{W} from low resolution MRS data to high resolution anatomical data for spatial normalization across study participants. Figure 2 shows a representative spectrum in a voxel of the MPCSI dataset.

[Figure 2]

Spatial Normalization of MPCSI Data MPCSI data for each participant were coregistered into the coordinate space of a T1-weighted image of a template brain. Specifically, each participant's localizer image was coregistered to its high-resolution T1w image using a similarity transformation (3 translations and 3 rotations) such that the transformation maximized mutual information (Viola, 1995) across the localizer and its corresponding high resolution T1w image. Second, we spatially transformed the localizer image using the similarity transformation that coregistered the T1w image of the participant into the coordinate space of the template brain. Third, we warped the coregistered localizer by applying to it the high-dimension, nonlinear deformation that warped the participant T1w image to the template T1w image. We applied these 3 coregistration procedures to each of the metabolite images.

The MPCSI saturation bands applied to suppress lipid signal from the scalp were not as precisely shaped as the scalp, and they unavoidably suppressed metabolite signals from several portions of cortical gray matter. Moreover, lipid signal from the small portions of scalp that were unsuppressed contaminated MRS signal to some degree within the brain, and those voxels were censored from further analyses during the detailed visual inspection of the spectra recorded from each of the 8 channels of the multi-channel head coil. Consequently, metabolite measures for many participants were available only in voxels of WM and deep gray matter

nuclei. We show in each metabolite map a gray scale image representing the number of participants who had usable data at each voxel. We suppressed display of results at any voxel that did not have usable data from at least half the participants.

Statistical Analyses

Age Correlates of DTI and MPCSI Measures We hypothesized that increasing age would be associated with differences in cerebral microstructure (FA, ADC) and neurometabolite concentrations (NAA) in CTSC pathways, representing progressively advancing brain maturation within our primary cohort of children ages 9-12. To test these hypotheses, we used voxel-wise multiple linear regression models in MATLAB (MATLAB, RRID:SCR_001622) using inhouse generated programs to assess the association of age with DTI (FA and ADC) and MPCSI (NAA) measures entered separately as dependent variables, age entered as the independent variable, and sex as a covariate.

Mediation Analyses We assessed whether our imaging measures mediated the association of age with measures of psychometric performance. These analyses would only be meaningful when applied to psychometric variables that correlated significantly with age. Therefore, we assessed mediation only for those performance raw scores (i.e., unadjusted for age) that correlated significantly with age while controlling for sex. Raw scores that were highly skewed were transformed using an inverse hyperbolic sine: $ihs(x) = \log\left[x + \sqrt{x^2 + 1}\right]$ (Burbridge et al., 1988). Of the raw performance scores that correlated significantly with age, only NEPSY Inhibition/Switching and CPT Hit Reaction Time scores sufficiently normalized to provide stable mediation estimates and entered mediation analyses along with Design Copy scores, which did not require transformation. We then calculated the statistical significance of the brain imaging values (variable M) mediating the association between age (independent variable X), and psychometric scores (dependent variable Y), using 3 regression equations: 1) $Y = c_1X + e_1$, which examines the unadjusted association of age with psychometric score; 2) $M = aX + e_2$,

383 which examines the association of age with the brain mediator; and 3) $Y = c_2X + bM + e_3$, which
384 examines the association of age with psychometric score adjusting for the mediator. Sex was
385 included as a covariate in all three equations. As noted above, we first assessed whether the
386 independent variable (age) was significantly associated with the dependent variable (raw
387 performance scores); we also assessed whether the independent variable (age) was
388 significantly associated with the mediating variable (imaging measures). If both of these
389 associations were significant, we then tested whether the indirect effect $a\ x\ b$ differed
390 significantly from zero using a z-score, $z_{ab} = (a\ x\ b)/se_{ab}$, where $se_{ab} =$
391 $\sqrt{(a^2\ x\ se_b^2) + (b^2\ x\ se_a^2)}$, and se_a, se_b were the standard errors of the regression coefficients a
392 and b, respectively (MacKinnon, 2008). Significant mediating effect suggests that association of
393 X with Y in regression (1) is weakened by M in regression (3).
394 Post Hoc Analyses We conducted several post hoc tests to aid interpretation of findings from a
395 priori hypothesis testing. For example, we performed linear regression using AD and RD as the
396 dependent variables to interpret better the microstructural features likely generating the age
397 correlations for FA and ADC. Similarly, linear regressions using Ch, Cr, and Glx as dependent
398 variables aided interpretation of age correlates for NAA in terms of membrane turnover (Ch),
399 energy metabolism (Cr), or neurotransmission (Glx). Additional post hoc analyses included age
400 correlations and mediation analyses for the entire cohort of 309 participants, aged 5-14 years, to
401 assess whether findings in the restricted age range of 9-12 years obtained across a wider
402 developmental window. We also performed regression analyses with family income, maternal
403 hardship, and ethnicity entered as additional covariates to ensure that our findings were not
404 attributable to possible confounds in this sample of participants. Finally, we generated
405 scatterplots of significant correlations of age with brain imaging and psychometric measures to
406 provide further assurance that findings were not spurious or generated by statistical outliers,
407 and to assess whether age correlates contained any curvilinear effects.

Statistical Parametric Maps and Correction for Multiple Comparisons We used a method for False Discovery Rate (FDR) to control for multiple comparisons across all the voxels within each statistical map. We further corrected p-values for the 5 statistical tests of our a priori hypotheses, to establish an overall *p*-value <0.05 study-wide. Thus, we required the 5 maps that tested our 5 a priori hypotheses to yield an FDR $p < 0.01$. Furthermore, we eliminated regions with fewer than 100 significant voxels, assuming them to be less reproducible and biologically less important. We applied morphological operators of dilation followed by erosion, each two voxels wide, to fill two voxel-wide holes in thresholded p-value maps. P-values <0.01 that survived FDR correction were color-coded and plotted on brain images such that warm colors (red/orange) represented positive associations and cool colors (blue shades) indicated inverse associations.

We note that application of the FDR procedure across MRS and DTI data, resampled to the 557,200 voxels of the high-resolution anatomical image, in itself provides a stringent and conservative control for false positives in our findings because the measures were highly correlated across voxels. We acquired the MRS data, for example, on a 24x24 grid in each of the 6 axial-oblique slices parallel to the AC-PC line. The nominal, within-slice resolution was 10 x 10 mm^2, with 10 mm slice thickness. The signal from an MRS voxel within a slice, however, was dispersed into its neighboring voxels with a point spread function (PSF) having a full width at half maximum (FWHM) of 30 mm, yielding a total of 6*(240*240)/(30*30)=384 independent resolution elements (RESELs). Therefore, although we needed to control for fewer than 400 independent statistical tests for the MRS data, we applied the FDR procedure to 557,200 voxels to provide added confidence in the validity of our findings.

Results

Demographic data for both the 9-12 and 5-14 year old age groups are presented in Table 1. Participants were exclusively racial/ethnic minorities and of lower to middle socioeconomic status.

[Table 1]

A comparison of demographic data by imaging modality (participants with usable DTI, MRS, or both DTI and MRS) for both age cohorts is shown in Table 2.

[Table 2]

Age Correlations with DTI Measures

Fractional Anisotropy (**FA**)

White matter: FA correlated positively with age in deep white matter fiber bundles such as the corona radiata, posterior limb of the internal capsule, superior longitudinal fasciculus, posterior thalamic radiation (TR), and cerebral peduncles, as well as in superficial cortical white matter within prefrontal and parietal regions (Fig 3A). The TR and superior longitudinal fasciculus (SLF) are deep white matter fiber tracts that integrate information across distant and disparate brain regions – anterior to posterior brain regions for the SLF, and from cortex to thalamus and brainstem for the TR.

Gray matter: FA correlated positively with age in the anterior and posterior cingulate cortices, superficial cortical gray matter, lenticular nucleus, caudate, thalamus, midbrain, medial occipital cortex, and cerebellum (Fig 3A).

Apparent Diffusion Coefficient **(ADC)**

White matter: ADC correlated inversely with age in the corona radiata, centrum semiovale, superior longitudinal fasciculus, thalamic radiation, and extreme capsule, as well as in superficial cortical white matter in the prefrontal cortex (PFC) (Fig 3A).

Gray matter: ADC correlated inversely with age in subcortical gray matter including the lenticular nucleus and thalamus, and in the posterior cingulate cortex and midbrain (Fig 3A).

Post Hoc Analyses

RD and AD: The similarity in RD maps to ADC maps, and the minimal correlations of age with AD for both white and gray matter, indicate that age-related changes in the radial direction of diffusion accounted for correlations of age with ADC (Fig 3A).

Extended Age Range: DTI findings in GM were consistent across the 9-12 and 5-14 year old cohorts, though they appeared somewhat stronger in WM in the 5-14 year olds (Fig. 3B).

[Figure 3]

Age Correlations with Metabolite Concentrations

NAA

White matter: NAA correlated with age in the dorsolateral PFC (dlPFC) and inversely with age in the parietal WM (Fig 4A).

Gray matter: NAA correlated positively with age in the dorsal anterior cingulate cortex (ACC), insula and thalamus, and inversely in the medial occipital GM (Fig 4A).

Post Hoc Analyses

Ch

White matter: Ch correlated inversely with age in the PLIC, dlPFC, and parietal and occipital WM (Fig 4A).

Gray matter: Ch correlated positively with age in the pregenual and dorsal ACC, caudate, and insular cortex (Fig 4A).

Cr

White matter: Cr correlated inversely with age in the posterior limb of the internal capsule, thalamic radiation, and parietal WM (Fig 4A).

Gray matter: Cr correlated positively with age in the dorsal ACC and insular cortex, and inversely in the thalamus (Fig 4A).

Glx

White matter: Glx correlated inversely with age in the posterior limb of the internal capsule, external capsule, angular gyrus, corona radiata, superior longitudinal fasciculus, and thalamic radiation (Fig. 4A).

Gray matter: Glx correlated positively with age in the insular cortex, caudate, and ACC (Fig. 4A).

Extended Age Range: The MRS findings in both WM and GM were similar in the 5-14 year olds, except for stronger inverse correlations of age with Ch concentrations in deep WM (Fig. 4B).

[Figure 4]

Brain Measures Mediating the Association of Age with Cognitive Performance We assessed whether brain imaging measures mediated the association of age with measures of performance on self-regulatory tasks, testing mediation only for those cognitive variables that correlated significantly with age (Table 3). Notably, all raw error scores and CPT Hit Reaction Time correlated significantly and inversely with age, thus indicating that increasing age was associated with decreasing errors and shorter reaction times, representing improved performance. CPT Hit Reaction Time Detectability and NEPSY Design Copy scores correlated positively with age, signifying improved performance with age.

[Table 3]

Fractional Anisotropy (FA) FA significantly mediated the associations of age with the NEPSY Design Copy Process Global scores and CPT Hit Reaction Time. The number of participants varied slightly among different measures, as noted in Figures 5 and 6, because not every participant with imaging completed each psychometric measure. Increased FA in GM of the thalamus and caudate, and WM of the internal capsule and splenium of the corpus callosum partially mediated the association of age with better scores on the Process Global subscale of the Design Copy task, which requires both visuospatial processing skills and executive functioning (Fig. 5A). Higher FA in the lenticular nucleus and thalamus, but also in the IFOF, internal capsule, and splenium of the corpus callosum partially mediated the association of

increasing age with better performance (demonstrated as lower scores, or shorter Hit Reaction Times) on the CPT (Fig. 5A).

Post Hoc Analyses In the 5-14 year olds, mediation of FA with age in CPT Hit Reaction Time was significant in all areas but the IFOF, and in Design Copy was significant in the CCsp and caudate (Fig. 5B).

[Figure 5]

NAA NAA in the thalamus partially mediated the association of age with improving performance (shorter Hit Reaction Times) on the CPT (Fig 6A).

Post Hoc Analyses The NAA mediation finding in the thalamus was not detected in the 5-14 year olds (Fig. 6B).

Glx Glx in the WM of the putamen and external capsule partially mediated the association of age with improved performance on the CPT (Fig. 6C), and mediation in the putamen was also significant in the full cohort (Fig. 6D).

[Figure 6]

Diagrams of each mediation with scatterplots of representative brain regions are shown for FA (Fig. 7) and for NAA and Glx (Fig. 8), demonstrating age correlates that vary monotonically and positively with increasing age, without evidence of curvilinear effects. FA mediation of the association of age with CPT Hit Reaction Time in the restricted age group was significant in the PLIC at p = 0.00001, unstandardized beta = -0.0003 (95% confidence interval: -0.0004, -0.0002, effect size = -2.99) (Fig. 7A, upper). In the full cohort, mediation was significant at p = 0.0002, unstandardized beta = -0.0002 (95% confidence interval: -0.0003, -0.0001, effect size -2.65 [Cohen's d effect size computed by dividing the mean of the mediation effect by its standard deviation]) (Fig. 7B, upper). FA mediation of age correlates with Design Copy in the restricted age group was significant in the caudate at p = 0.01, unstandardized beta = 0.005 (95% confidence interval: 0.001, 0.01, effect size = 1.61) (Fig. 7A, lower); and was also

significant in the expanded age group at $p = 0.01$, unstandardized beta = 0.004 (95% confidence interval: 0.001, 0.008, effect size = 2.11) (Fig. 7B, lower).

NAA mediation of the age correlate with CPT Hit Reaction Time was significant in the thalamus in the limited age cohort at $p = 0.02$, unstandardized beta = 0.0002 (95% confidence interval 0.00003, 0.0003, effect size = 1.82) (Fig. 8A, upper), but there was no brain region finding of NAA mediation in the expanded cohort (Fig. 8B, upper). Glx mediation of age correlates with CPT Hit Reaction Time was significant in the putamen in both the 9-12 year cohort [$p = 0.05$, unstandardized beta = 0.0004 (95% confidence interval: 0.00001, 0.0007, effect size = -1.48)] (Fig. 8A, lower) and full cohort [$p = 0.05$, unstandardized beta = 0.0003 (95% confidence interval: 0.000004, 0.0007, effect size = -1.55)] (Fig. 8B, lower).

[Figures 7 & 8]

Discussion

The transition from childhood to adolescence is characterized by an increasing ability to self-regulate thought, emotion, and behavior. Using voxel-wise analyses of DTI and MPCSI data, we have shown that this period is also characterized by maturational correlates in microstructure and metabolites, most prominently in frontal and cingulate cortices, striatum, thalamus, WM, and cerebellum. Our results also show that maturational correlates in the striatum, thalamus, and WM partially mediate performance improvements in preadolescent children. These findings generally held true in post hoc analyses of an expanded cohort 5-14 years of age.

White Matter Maturation Increasing age was associated with increasing FA and decreases in ADC and RD across large sectors of frontal WM, extending from the centrum semiovale to deep WM, and anteriorly to the frontal pole (Fig. 3). We found little evidence for age-related decreases in ADC, RD, or AD in parietal or occipital WM.

Strong positive associations of age with higher FA values, and inverse associations of age with ADC and RD values, with little contribution from AD, suggest that cellular maturation

disproportionately reduces diffusion in the radial direction of fiber bundles. The most obvious possible explanations for these findings include age-related increases in myelination or axon packing density. Myelination restricts radial diffusion in axons, primarily because myelin is highly hydrophobic (Stoffel et al., 1984); increasing myelination with age would reduce ADC and RD, and increase FA. Greater axon packing density would yield more plasma membranes, myelin, and cell organelles, and less extracellular water, reducing RD and possibly increasing FA (Beaulieu, 2002).

Prior studies in children and adolescents reported age-related decreases in ADC and RD (Lebel et al., 2008; Colby et al., 2011; Simmonds et al., 2014) and age-related increases in FA (Barnea-Goraly et al., 2005) in WM. These maturational changes, thought to reflect ongoing myelination (Yakovlev and Lecours, 1967; Colby et al., 2011), appear to follow a posterior-to-anterior temporal gradient. Our findings are consistent with these reports across a much narrower age-range (9-12 years), and they demonstrate, for the first time, that associations of age with microstructure are *not* accompanied by age-related alterations in WM metabolite concentrations (Fig. 4).

This observation differs markedly from the close association of myelination with metabolite concentrations observed earlier in development (Bluml et al., 2013). Although unexpected, the absence of significant age correlates in WM metabolite concentrations, together with significant age correlations in WM microstructure, has at least two possible explanations. First, transient variation of metabolite concentrations during this developmental period could be missed by our linear models and cross-sectional study design. Second, WM microstructure development during this period may not require substantial metabolite alterations.

Myelin forms when an oligodendrocyte wraps an axon with a flattened cytoplasmic process. Over time, that process loses its cytoplasmic content to form a much more compact, tightly wound, membranous sheath of alternating lipid and protein laminae (Raine, 1984). After

584 myelin synthesis peaks, protein and lipid synthesis in myelin decline rapidly (Benjamins and
585 Smith, 1984), though slow turnover of the constituent myelin lipids and proteins, and activity-
586 dependent remodeling of myelin, continues across the lifespan (Smith, 1968; Uzman and
587 Hedley-Whyte, 1968; Nave, 2010; Young et al., 2013; Gibson et al., 2014; Yeung et al., 2014).
588 Accordingly, our findings of an age-related decline in RD and increase in FA, coupled with
589 stable WM metabolites are consistent with remodeling of myelin, perhaps into a more compact
590 structure, during the transition from childhood to adolescence.
591 **Gray Matter Maturation** Increasing age was associated with higher FA values in prefrontal,
592 insular, anterior temporal, inferior parietal, and cingulate cortices, as well as basal ganglia,
593 thalamus, and cerebellum (Fig.3). We found little evidence for FA age correlates in posterior
594 temporal, parietal, or occipital cortices. Neuronal components of GM consist primarily of cell
595 bodies, dendritic and axon terminal arbors, and synapses, all with generally less directional
596 orientation than in WM, and GM axon segments are mostly unmyelinated. Most neurons and
597 glia in subcortical GM nuclei, and in some cortical layers, are stellate in shape, further reducing
598 overall directional diffusion of intracellular water. Nevertheless, many neurons and glia in the
599 cortex are oriented perpendicular to the cerebral surface, which can produce a directional
600 coherence in diffusion. Thus, even though DTI studies often exclude FA values < 0.2 to mask
601 GM, FA and other DTI indices in GM are valid and worth study, especially in larger sample sizes
602 that can overcome the restricted range of DTI indices and lower signal-to-noise in GM (Farrell et
603 al., 2007).
604 Age-related increases in FA and reductions in ADC and RD in GM, could derive from
605 age-related increases in myelination of WM fibers entering or exiting GM (Lebel et al., 2008), or
606 in the thalamus, from myelinated dendritic spines of medium spiny neurons (Rafols et al., 1989).
607 Alternatively, an age-related increase in cell packing density could produce these findings, as
608 FA correlates strongly with the number of non-myelinated axons in each voxel (Leong et al.,
609 2015); presumably, this would be true not only for increased GM density of neurons and glia,

but also for increased GM density of dendritic arbors and synapses in. Although prior morphological imaging studies have shown that frontal, temporal, and parietal GM, and GM of the basal ganglia and thalamus, mature throughout late childhood and adolescence (Giedd et al., 1999; Sowell et al., 2003; Shaw et al., 2008; Raznahan et al., 2014; Walhovd et al., 2017), our findings extend these observations to GM microstructure.

We also show, for the first time, variations in GM metabolite concentrations with advancing age. NAA and creatine are key compounds involved in energy metabolism (Chakraborty et al., 2001), and NAA and choline participate in lipid synthesis. Higher NAA concentrations generally reflect increased mitochondrial energy metabolism, increased demand for lipid synthesis, or increased NAAG. Therefore, the observed age-related GM increases in NAA, creatine, or choline in GM suggest structural or functional growth in these locations, especially dendritic arborization and synaptogenesis, whereas decreases in NAA, creatine, and choline in parieto-occipital cortices suggest dendritic or synaptic pruning.

Microstructure and Metabolism Mediate Age-Related Improvements in Cognitive Performance FA values in the internal capsule, basal ganglia, and thalamus partially mediated associations of increasing age with shorter reaction times on the CPT and improved performance on Design Copy (Fig. 5). Higher NAA concentrations in the thalamus also partially mediated age-related improvement in CPT reaction times (Fig. 6). Each of these mediation findings had a large effect size, underscoring the robustness of the mediation. These mediation findings suggest that microstructural maturation of the basal ganglia, thalamus, and WM of the internal capsule play central roles in improving performance capacity during the transition from childhood to adolescence. The internal capsule densely interconnects the basal ganglia and thalamus with frontal cortex, which together constitute CSTC circuits. These circuits comprise largely parallel projections from specific cortical regions to the basal ganglia/substantia nigra, then to thalamus, and back to the cortical regions from which the projections originated. They include two separate but interacting pathways: one, the “direct” or excitatory pathway, connects

636 the striatum to the globus pallidus interna/substantia nigra (GPi/SN) complex to generate “go”
637 signals for behavior; the other, an “indirect” pathway, connects the striatum to the globus
638 pallidus externa and subthalamic nucleus, then to the GPi/SN, to generate “stop” signals that
639 serve as a “brake” on the direct pathway and impulses to action (Mink, 1996; Tekin and
640 Cummings, 2002). Balance of activity in these pathways modulates output from the striatum to
641 the thalamus and consequently the output from the thalamus to the cortex. This intricate
642 organization of CSTC circuits positions them to serve as powerful modulating influences on
643 thought, emotion, and behavior. Thus, our findings suggest that maturation of the basal ganglia,
644 thalamus, and WM of the frontal lobes and internal capsule within CSTC circuits supports
645 development of cognitive and self-regulatory capacities during the transition from late childhood
646 into early adolescence.
647 **Limitations** (1) Inferences about developmental trajectories must be made cautiously in cross-
648 sectional studies such as ours. A prospective longitudinal study with multiple imaging time
649 points is needed to conclusively identify developmental trajectories for white and gray matter
650 maturation during this period. It would also permit analyses of within-subject change in imaging
651 measures and cognitive performance, affording more powerful analyses of brain-based
652 mediation of the cognitive and behavioral capacities that emerge in preadolescence. (2)
653 Pubertal status was not assessed concurrently at the time of MRI scanning, precluding an
654 attempt to disentangle the effects of pubertal development and age on our findings. (3) Ours
655 was a sample of urban and racial/ethnic minority participants and therefore, our findings may
656 not generalize to other populations.
657 **Conclusions** Our findings of this study suggest a rapid maturation of CSTC pathways during
658 the developmental transition from childhood to adolescence. Maturation of those pathways
659 partially mediates the emergence of greater capacities for self-regulation at a time of increasing
660 academic and social demands. Having defined the normative features of tissue organization
661 and metabolism will permit future study of the ways in which aberrant development of CTSC

662 pathways may support the emergence of behavioral disorders in adolescence that feature
663 impaired self-regulatory control.

664 **References**

665 Alexander AL, Lee JE, Lazar M, Field AS (2007) Diffusion tensor imaging of the brain.
666 Neurotherapeutics 4:316-329.
667
668 Barnea-Goraly N, Menon V, Eckert M, Tamm J, Bammer R, Karchemsky A, Dant CC, Reiss AL
669 (2005) White matter development during childhood and adolescence: a cross-sectional
670 diffusion tensor imaging study. Cereb Cortex 15:1848-1854.

671 Beaulieu C (2002) The basis of anisotropic water diffusion in the nervous system - a technical
672 review. NMR in Biomedicine 15.

673 Benjamins JA, Smith ME (1984) Metabolism of myelin. In: Myelin (Morell P, ed). Boston, MA:
674 Springer.

675 Bluml S, Wisnowski JL, Nelson MD, Jr., Paquette L, Gilles FH, Kinney HC, Panigrahy A (2013)
676 Metabolic maturation of the human brain From birth through adolescence:iInsights from
677 in vivo magnetic resonance spectroscopy. Cereb Cortex 23:2944-2955.

678 Burbridge JB, Magee L, Robb AL (1988) Alternative transformations to handle extreme values
679 of the dependent variable. J Am Stat Assoc 83:123-127.

680 Cercignani M, Inglese M, Pagani E, Comi G, Filippi M (2001) Mean diffusivity and fractional
681 anisotropy histograms of patients with multiple sclerosis. Am J Neuroradiol 22:952-958.

682 Chakraborty G, Mekala P, Yahya D, Wu G, Ledeen RW (2001) Intraneuronal N-acetylaspartate
683 supplies acetyl groups for myelin lipid synthesis: evidence for myelin-associated
684 aspartoacylase. J Neurochem 78:736-745.

685 Christensen GE, Rabbitt RD, Miller MI (1994) 3D brain mapping using a deformable
686 neuroanatomy. Phys Med Biol 39:609-618.

687 Colby JB, Van Horn JD, Sowell ER (2011) Quantitative *in vivo* evidence for broad regional
688 gradients in the timing of white matter maturation during adolescence. Neuroimage
689 54:25-31.

690 Colibazzi T, Zhu H, Bansal R, Schultz R, Peterson BS (2008) Latent volumetric structure of the
691 human brain: exploratory factor analysis and structural equation modeling of gray matter
692 volumes in healthy children and adults. Hum Brain Mapp 29:1302-1312.

693 Conners CK (1994) The Connors Continuous Performance Test (CPT): Computer Program,
694 Version 3.0. North Tonawanda: Multi-Health Systems, Inc.

695 Dong ZC, Peterson B (2007) The rapid and automatic combination of proton MRSI data using
696 multi-channel coils without water suppressionl. Magnetic Resonance Imaging 25:1148-
697 1154.

698 Dubin MJ, Maia TV, Peterson BS (2010) Cognitive control in the service of self-regulation. In:
699 The Encyclopedia of Behavioral Neuroscience (Koob GF, Le Moal M, Thompson RF,
700 eds). Amsterdam, Netherlands: Elsevier.

701 Farrell JA, Landman BA, Jones CK, Smith SA, Prince JL, Van Zijl PCM, Mori S (2007) Effects of
702 SNR on the accuracy and reproducibility of DTI-derived fractional anisotropy, mean

703 diffusivity, and principal eigenvector measurements at 1.5T. J Magn Reson Imaging
704 26:756-767.

705 Gibson EM, Purger D, Mount CW, Goldstein AK, Lin GL, Wood LS, al. E (2014) Neuronal
706 activity promotes oligodendrogenesis and adaptive myelination in the mammalian brain.
707 Science 344:1252304.

708 Giedd JN, Blumenthal J, Jeffries NO, Castellanos FX, Liu H, Zijdenbos AP, Paus T, Evans AC,
709 Rapoport JL (1999) Brain development during childhood and adolescence: a longitudinal
710 MRI study. Nat Neurosci 2:861-863.

711 Goncalves OF, Carvalho S, Liete J, Fernandes-Goncalves A, Carracedo A, Sampaio A (2016)
712 Cognitive and emotional impairments in obsessive-compulsive disorder: evidence from
713 functional brain alterations. Porto Biomed J 1:92-105.

714 Hao X, Xu D, Bansal R, Dong Z, Liu J, Wang Z, Kangarlu A, Liu F, Duan Y, Shova S, Gerber
715 AJ, Peterson BS (2013) Multimodal magnetic resonance imaging: The coordinated use
716 of multiple, mutually informative probes to understand brain structure and function. Hum
717 Brain Mapp 34:253-271.

718 Haselgrove JC, Moore JR (1996) Correction for distortion of echo-planar images used to
719 calculate the apparent diffusion coefficient. Magnetic Resonance in Medicine 36:960-
720 964.

721 Jauregui-Lobera I (2016) Neuroimaging in eating disorders. Neuropsychiatr Dis Treat 7:577-
722 584.

723 Jenkinson M, Bannister P, Brady M, Smith S (2002) Improved optimization for the robust and
724 accurate linear registration and motion correction of brain images. Neuroimage 17:825-
725 841.

726 Kemp S, Korkman M, Kirk U (2007) Developmental Neuropsychological Assessment, Second
727 Edition (NEPSY-II). In: Pearson, Inc.

728 Kessler RM, Hutson PH, Herman BK, Potenza MN (2016) The neurobiologic basis of binge-
729 eating disorder. Neurosci Biobehav Rev 63:223-238.

730 Lebel C, Walker L, Leemans A, Phillips L, Beaulieu C (2008) Microstructural maturation of the
731 human brain from childhood to adulthood. Neuroimage 40:1044-1055.

732 Lebon V, Petersen KF, Cline GW (2002) Astroglial contribution to brain energy metabolism in
733 humans revealed by 13C nuclear magnetic resonance spectroscopy: elucidation of the
734 dominant pathway for neurotransmitter glutamate repletion and measurement of
735 astrocytic oxidative metabolism. J Neurosci 22:1523-1531.

736 Leong D, Calabrese E, White LE, Wei P, Chen S, Platt SR, Provenzale JM (2015) Correlation of
737 diffusion tensor imaging parameters in the canine brain. The Neuroradiology Journal
738 28:12-18.

739 Leung HC, Skudlarski P, Gatenby JC, Peterson BS, Gore JC (2000) An event-related functional
740 MRI study of the stroop color word interference task. Cereb Cortex 10:552-560.

741 MacKinnon DP (2008) Introduction to Statistical Mediation Analysis. New York: Lawrence
742 Erlbaum Associates.

743 Marsh R, Maia TV, Peterson BS (2009a) Functional disturbances within frontostriatal circuits
744 across multiple childhood psychopathologies. Am J Psychiatry 166:664-674.

745 Marsh R, Zhu H, Wang Z, Skudlarski P, Peterson BS (2007) A developmental fMRI study of
746 self-regulatory control in Tourette's syndrome. Am J Psychiatry 164:955-966.

747 Marsh R, Steinglass JE, Gerber AJ, O'Leary KG, Walsh BT, Peterson BS (2009b) Deficient
748 activity in the neural systems that mediate self-regulatory control in bulimia nervosa.
749 Arch Gen Psychiatry 66:1-13.

750 Mink JW (1996) The basal ganglia: focused selection and inhibition of competing motor
751 programs. Prog Neurobiol 50:381-425.

752 Mukherjee P, Miller JH, Shimony JS, Philip JV, Nehra D, Snyder AZ, Conturo TE, Neil JJ,
753 McKinstry RC (2002) Diffusion-tensor MR imaging of gray and white matter development
754 during normal human brain maturation. Am J Neuroradiol 23:1445-1456.

755 Nave KA (2010) Myelination and support of axonal integrity by glia. Nature 468:244-252.

756 Nigg JT (2016) Annual Research Review: on the relations among self-regulation, self-control,
757 executive functioning, effortful control, cognitive control, impulsivity, risk-taking, and
758 inhibition for developmental psychopathology. J Child Psychol Psychiatry.

759 Pavuluri MN, S. Y, Kamineni K, Passarotti AM, Srinivasan G, Harral EM, Sweeney JA, Zhou XJ
760 (2009) Diffusion tensor imaging study of white matter fiber tracts in pediatric bipolar
761 disorder and attention-deficit/hyperactivity disorder. Biol Psychiatry 65:586-593.

762 Peterson BS, Skudlarski P, Gatenby JC, Zhang H (1999) An fMRI Study of Stroop Word-Color
763 interference: evidence for cingulate subregions subserving multiple distributed
764 attentional systems. Biological Psychiatry 45:1237-1258.

765 Peterson BS, Kane MJ, Alexander GE, Lacadie C (2002) An event-related functional MRI study
766 comparing interference effects in the Simon and Stroop tasks. Cognitive Brain Research
767 13:427-440.

768 Peterson BS, Thomas P, Kane MJ, Scahill L, Zhang H, Bronen R, King RA, Leckman JF, Staib
769 LH (2003) Basal ganglia volumes in patients with Gilles de la Tourette syndrome. Arch
770 Gen Psychiatry 60:415-424.

771 Power JD, Barnes KA, Snyder AZ, Schlaggar BL, Petersen SE (2012) Spurious but systematic
772 correlations in functional connectivity MRI networks arise from subject motion.
773 NeuroImage 59:2142-2154.

774 Rae CD (2014) A guide to the metabolic pathways and function of metabolites observed in
775 human brain ^{1}H magnetic resonance spectra. Neurochem Res 39:1-36.

776 Rafols JA, Cheng HW, McNeill TH (1989) Golgi study of the mouse striatum: age-related
777 dendritic changes in different neuronal populations. J Comp Neurol 279:212-227.

778 Raine CS (1984) Morphology of myelin and myelination. In: Myelin (Morell P, ed). Boston, MA:
779 Springer.

780 Ramadan S, Lin A, Stanwell P (2013) Glutamate and glutamine: a review of *in vivo* MRS in the
781 human brain. NMR in Biomedicine 26.

782 Raznahan A, Shaw PW, Lerch JP, Clasen LS, Greenstein D, Berman R, Pipitone J, Chakravarty
783 MM, Giedd JN (2014) Longitudinal four-dimensional mapping of subcortical anatomy in
784 human development. Proc Natl Acad Sci U S A 111:1592-1597.

785 Rubia K (2011) "Cool" inferior frontostriatal dysfunction in attention-deficit/hyperactivity disorder
786 versus "hot" ventromedial orbitofrontal-limbic dysfunction in conduct disorder: a review.
787 Biol Psychiatry 69:e69-87.

788 Shattuck DW, Leahy RM (2002) BrainSuite: An Automated Cortical Surface Identification Tool.
789 Medical Image Analysis 8:129-142.

790 Shaw P, Kabani NJ, Lerch JP, Eckstrand K, Lenroot R, Gogtay N, Greenstein D, Clasen LS,
791 Evans A, Rapoport JL, Giedd JN, Wise SP (2008) Neurodevelopmental trajectories of
792 the human cerebral cortex. J Neurosci 28:3586-3594.

793 Simmonds D, Hallquist MN, Asato M, Luna B (2014) Developmental stages and sex differences
794 of white matter and behavioral development through adolescence: a longitudinal
795 diffusion tensor imaging (DTI) study. Neuroimage 92:356-368.

796 Smith ME (1968) Lipids and lipid metabolism. Biochim Biophys Acta.

797 Sowell ER, Peterson BS, Thompson PM, Welcome SE, Henkenius AL, Toga AW (2003)
798 Mapping cortical change across the human life span. Nat Neurosci 6:30-315.

799 Stoffel W, Hillen H, Giersiefen H (1984) Structural and molecular arrangement of proteolipid
800 protein of central nervous system myelin. Proc Natl Acad Sci U S A 81:5012-5016.

801 Tekin S, Cummings JL (2002) Frontal-subcortical neuronal circuits and clinical neuropsychiatry:
802 an update. J Psychosom Res 53:647-654.

803 Uzman BG, Hedley-Whyte T (1968) Myelin: dynamic or stable? J General Physiology 51:8-18.

804 Viola P, Wells, W. M. (1995) Alignment by Maximization of Mutual Information. In: IEEE Proc. of
805 the 5th Int. Conf. on Computer Vision, pp 16-23. Boston, MA.

806 Volkow ND, Koob GF, McLellan AT (2016) Neurobiologic advances from the brain disease
807 model of addiction. N Engl J Med 374:363-371.

808 Walhovd KB, Fjell AM, Giedd JN, Dale AM, Brown TT (2017) Through thick and thin: a need to
809 reconcile contradictory results on trajectories in human cortical development. Cereb
810 Cortex 27:1472-1481.

811 Yakovlev PL, Lecours AR (1967) The myelogenetic cycles of regional maturation of the brain.
812 In: Resional development of the brain in early life (Minkowski A, ed), pp 3-70. Oxford:
813 Blackwell.

814 Yeung MS, Zdunek S, Bergmann O, Bernard S, Salehpour M, Alkass K, al. E (2014) Dynamics
815 of oligodendrocyte generation and myelination in the human brain. Cell 159:766-774.

816 Young KM, Psachoulia K, Tripathi RB, Dunn SJ, Cossell L, Attwell D, al. E (2013)
817 Oligodendrocyte dynamics in the healthy adult CNS: evidence for myelin remodeling.
818 Neuron 77:873-885.

819

820 **FIGURE LEGENDS**

821 **Fig 1 – Age Histograms for (A) 9-12 and (B) 5-14 year old groups** The restricted age sample
822 (panel A) has a more uniform distribution, providing an improved representation of data across
823 this developmental period.

824 **Fig 2 - MR spectrum of sample voxel** Using a Lorentz-Gaussian line shape, principal
825 resonances were fit for *N*-acetyl-aspartate plus *N*-acetyl-aspartyl-glutamate (NAA; 2.0 ppm;
826 yellow), creatine plus phosphocreatine (Cr; 3.0 ppm; red), choline compounds (Ch; 3.2 ppm;
827 dark blue), and glutamine + glutamate (Glx; 2.3 ppm; purple), as well as contaminating lipids
828 (other colors). The quality of the spectra is excellent and signal-to-noise, especially for NAA, Cr,
829 and Ch, is high.

830 **Fig 3 – DTI Age Correlations** Axial brain diffusion tensor imaging (DTI) correlations with age,
831 controlling for sex with fractional anisotropy (FA) average reference slices at top. Panel A shows
832 findings in the 9-12 year old cohort, and panel B shows findings in the full 5-14 year old cohort.
833 False discovery rate (FDR) correction for multiple comparisons was applied with FDR at $p<0.01$.
834 Significant positive correlations ($p<0.01$) are indicated by warm colors (red, orange) and
835 significant inverse correlations are shown as cool colors (shades of blue). FA correlated with
836 age in the prefrontal cortex, deep white matter, subcortical gray matter, and cerebellum.
837 Apparent diffusion coefficient (ADC) and radial diffusivity (RD) correlated inversely with age in
838 bilateral thalami, prefrontal cortex, and temporal and frontal poles.

839 **Abbreviations** FA, fractional anisotropy; AD, axial diffusivity; ADC, apparent diffusion
840 coefficient; RD, radial diffusivity
841 ACC, anterior cingulate cortex; Cb, cerebellum; Cd, caudate; cing, cingulate gyrus; CP, cerebral
842 peduncles; CR, corona radiata; CS, centrum semiovale; EC, external/extreme capsule; IC,
843 internal capsule; IFG, inferior frontal gyrus; Ins, insular cortex; LN, lenticular nucleus; Mb,
844 midbrain; mOCC, medial occipital cortex; MTG, middle temporal gyrus; OFG, orbitofrontal

gyrus; PCC, posterior cingulate cortex; PFC, prefrontal cortex; PLIC, posterior limb of internal capsule; SLF, superior longitudinal fasciculus; SMG, supramarginal gyrus; STG, superior temporal gyrus; Th, thalamus; TR, thalamic radiation

Fig 4 – MPCSI Age Correlations Shown here are MPCSI metabolite correlations with age, controlling for sex, with anatomical reference slices at the top and maps indicating voxel-wise numbers of subjects at the bottom, with lighter shading indicating more subjects. Panel A shows results in the 9-12 year old cohort, while panel B shows results of the full 5-14 year old cohort. False discovery rate (FDR) correction for multiple comparisons was done with FDR at $p<0.01$. Significant positive correlations ($p<0.01$) are indicated by warm colors (red, orange) while significant inverse correlations are shown as cool colors (shades of blue). All metabolites, NAA, Cr, Ch, and Glx correlated with age in the ACC in both age groups. NAA additionally correlated with age in the dlPFC, insular cortex, and thalamus; and inversely correlated with age in the intraparietal sulcus and occipital gyrus. Ch correlated with age in the insular cortex and caudate, and inversely correlated with age in the occipital and angular gyri, thalamus, IPS and PLIC. Cr correlated with age in the caudate and insular cortex, and inversely correlated with age in the occipital and angular gyri, PCC, TR, thalamus, IPS and PLIC. Glx correlated with age in the insular cortex and caudate, and inversely with age in the posterior limb of the internal capsule, external capsule, corona radiata, angular gyrus, SLF, posterior cingulate cortex, and thalamic radiation.

Abbreviations NAA, n-acetylaspartate; Cr, creatine; Ch, choline; Glx, glutamate+glutamine; ACC, anterior cingulate cortex; AG, angular gyrus; CC, corpus callosum (body); CCg, genu of corpus callosum; Cd, caudate; CR, corona radiata; CS, centrum semiovale; dlPFC, dorsolateral prefrontal cortex; EC, external capsule; Ins, insular cortex; IPS, intraparietal sulcus; OG, occipital gyrus; PCC, posterior cingulate cortex; PLIC, posterior limb of internal capsule; SLF, superior longitudinal fasciculus; Th, thalamus; TR, thalamic radiation

Fig 5 – FA Mediation Shown here are axial brain images of FA mediating the associations of age with psychometric scores; FA correlations with age are shown at the top for ease of reference. Panel A shows findings in the 9-12 year old cohort; panel B shows findings in the 5-14 year old cohort. False discovery rate (FDR) correction for multiple comparisons was applied with FDR at $p<0.01$. Significant positive correlations ($p<0.01$) are indicated by warm colors (red, orange), and significant inverse correlations are shown as cool colors (shades of blue). Significant FA mediations of age were seen with Design Copy Process Global and Hit Reaction Time scores, most notably in the lenticular nucleus, thalamus, caudate, posterior limb of the internal capsule, corpus callosum and inferior fronto-occipital fasciculus.

Abbreviations FA, fractional anisotropy;
ACC, anterior cingulate cortex; ALIC, anterior limb of internal capsule; Cb, cerebellum; CCsp, splenium of corpus callosum; Cd, caudate; CR, corona radiata; IFG, inferior frontal gyrus; IFOF, inferior fronto-occipital fasciculus; Ins, insular cortex; LN, lenticular nucleus; Mb, midbrain; mOCC, medial occipital cortex; MTG, middle temporal gyrus; OFG, orbitofrontal gyrus; PCC, posterior cingulate cortex; PLIC, posterior limb of internal capsule; Put, putamen; SFOF, superior fronto-occipital fasciculus; SMG, supramarginal gyrus; STG, superior temporal gyrus; Th, thalamus

Fig 6 – NAA and Glx Mediation Shown are axial brain images of NAA and Glx mediating associations of age with psychometric scores, NAA/Glx correlations with age are shown at the top of panel A and C for ages 9-12, and mid-figure of panel B and D for ages 5-14, for reference. Significant mediation by NAA in the thalamus was found for the associations age with Hit Reaction Time scores in the 9-12 year age group, but not in the expanded 5-14 year old sample. Significant mediation by Glx in the putamen and external capsule was found for the associations of age with Hit Reaction Time scores in the 9-12 age group, and in the putamen in the expanded 5-14 year old sample.

Abbreviations NAA, n-acetylaspartate; Glx, glutamate+glutamine; EC, external capsule; Put, putamen; Th, thalamus

Fig 7 – FA Mediation with Scatterplots Shown here are illustrations of the mediating relationship of FA with age and behavioral measures. Representative scatterplots of sampled brain regions are shown for FA in children (**A**) 9-12 years old and (**B**) 5-14 years, where Beta is the degree of change in FA per unit change in age. All associations were statistically significant. In each panel, the scatterplot in the upper left shows the correlation of FA with age; that in the upper right shows the correlation of behavioral measure (CPT Hit Reaction Time or Design Copy Process score) with age; and that in the lower right shows the correlation of behavioral measure with FA. Effect size for panel A (upper) was -2.99 and for panel B (upper) was -2.65. Effect size for panel A (lower) was 1.61 and for panel B (lower) was 2.11.

Abbreviations FA, fractional anisotropy; Cd, caudate; PLIC, posterior limb of internal capsule

Fig 8 – NAA and Glx Mediation with Scatterplots Shown here are illustrations of the mediating relationship of NAA or Glx with age and behavioral measures. Representative scatterplots of sampled brain regions are shown for NAA and Glx in children (**A**) 9-12 years and (**B**) 5-14 years, where Beta is the degree of change in NAA or Glx per unit change in age. All associations were statistically significant, except for NAA mediation of the association with age with Hit Reaction Time in children ages 5-14. In each panel, the scatterplot in the upper left shows the correlation of NAA or Glx with age; that in the upper right shows the correlation of behavioral measure with age; and that in the lower right shows the correlation of behavioral measure with NAA or Glx concentration. Effect size for panel A (upper) was 1.82. Effect size for panel A (lower) was -1.48 and for panel B (lower) was -1.55.

Abbreviations NAA, n-acetylaspartate; Glx, glutamate+glutamine; Ins, insular cortex; Put, putamen; Th, thalamus

TABLE LEGENDS

Table 1 – **Demographics of Study Population**, including entire cohort of 309 children ages 5-14 and 280 children ages 9-12, with age of child at study, gender, race/ethnicity, WISC Full Scale IQ score, level of maternal education, and measure of maternal material hardship

Table 2 – Comparison of Study Population Demographics for entire cohort (309) and narrower age range cohort (280), based upon type of imaging completed – DTI, MRS, or both DTI and MRS

Table 3 – Significant Correlations of Neurocognitive Scores with Age to demonstrate those measures that were included in the mediation analyses, and the direction of association of age with each score

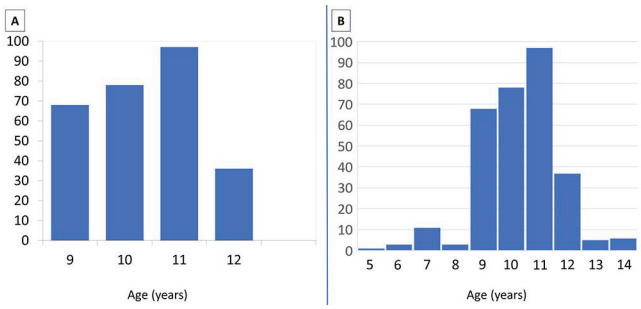

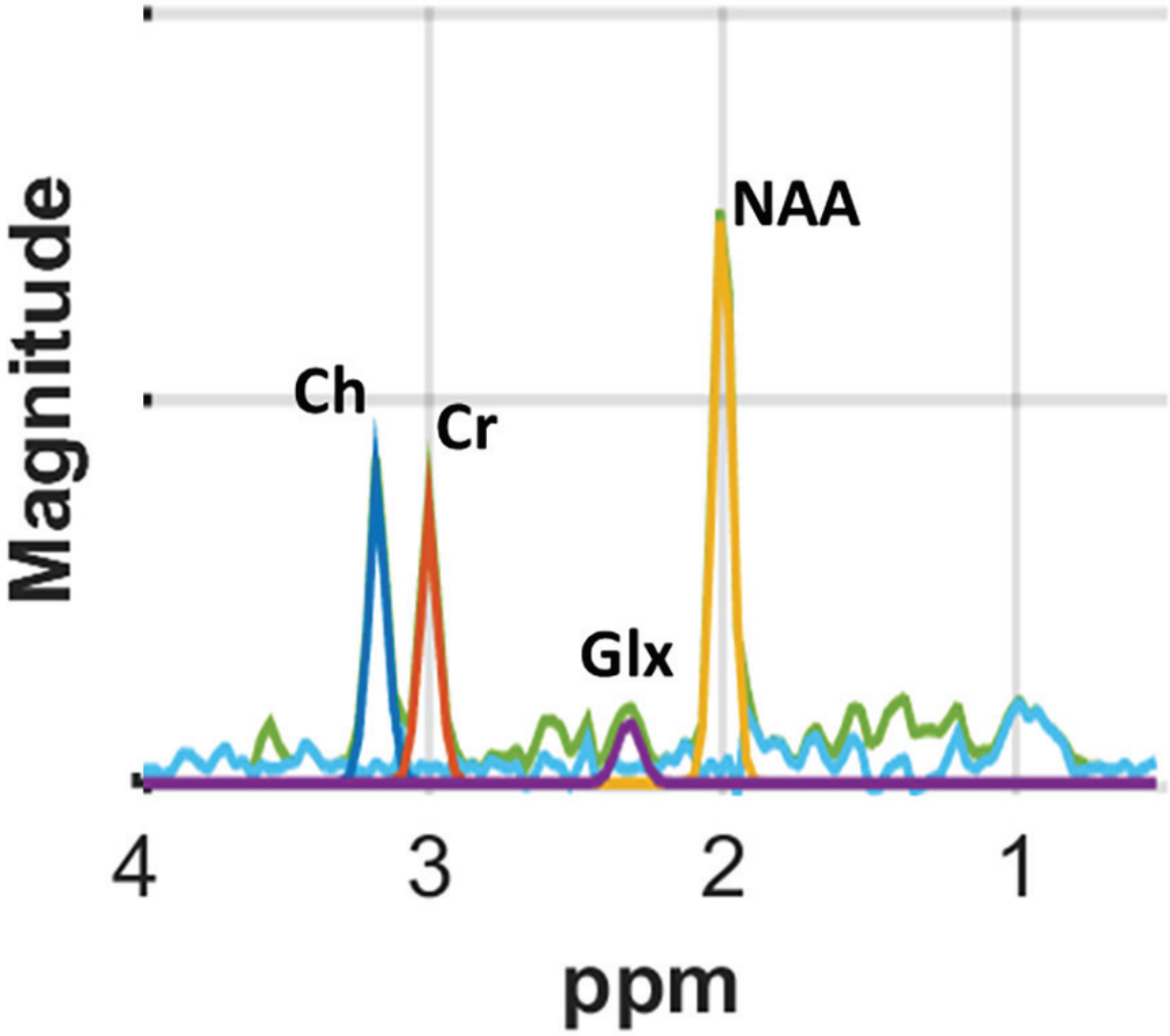

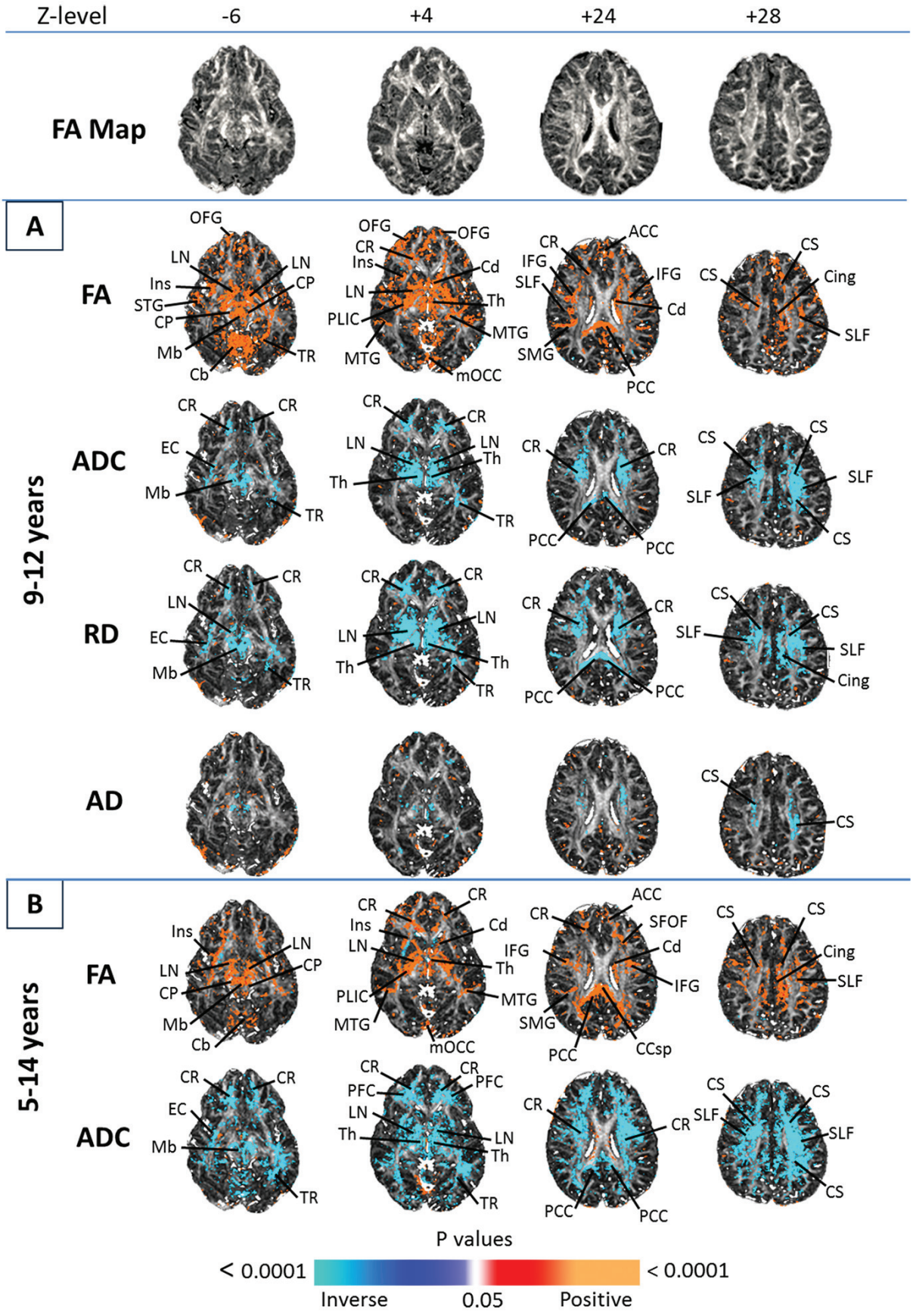

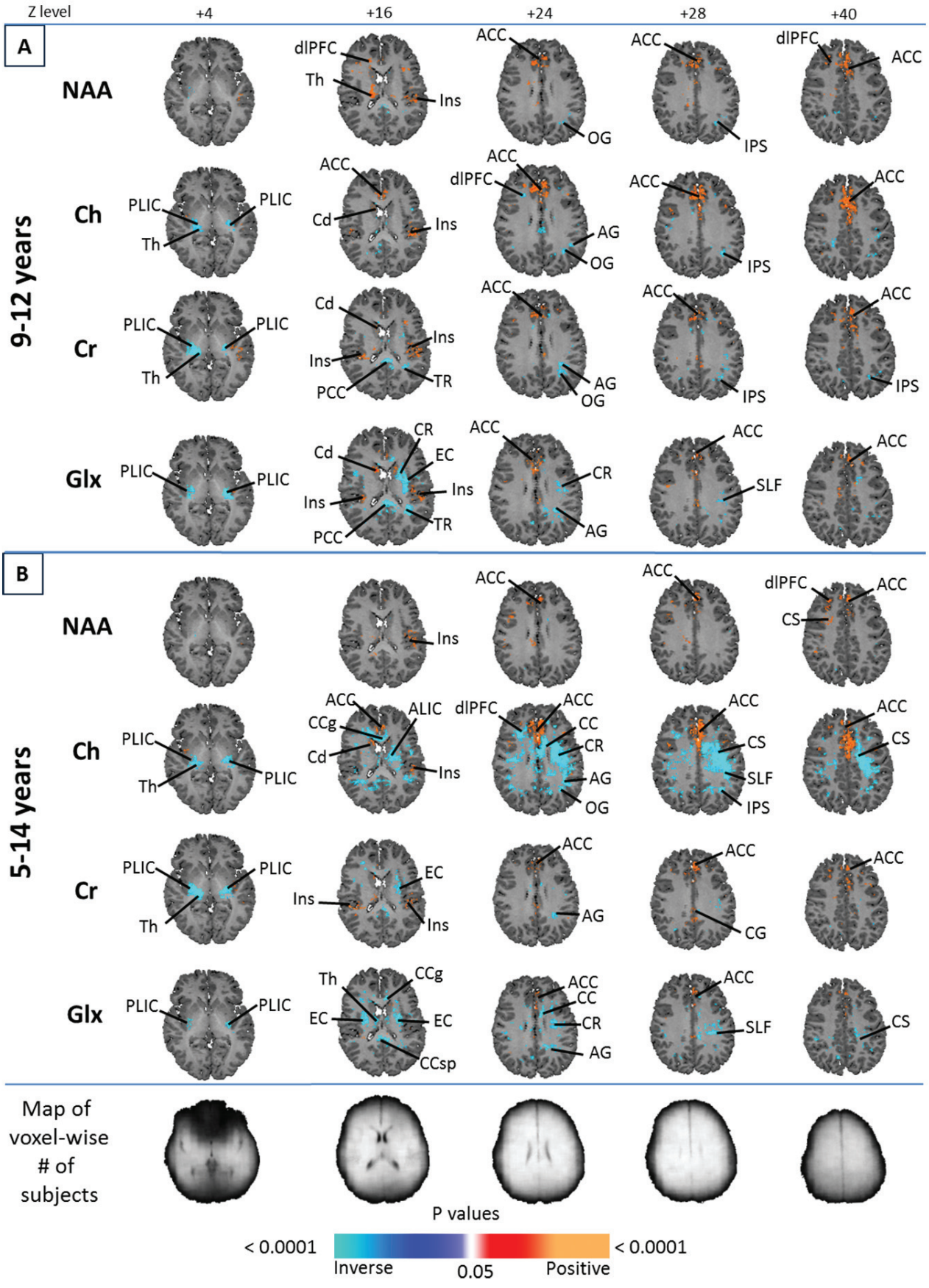

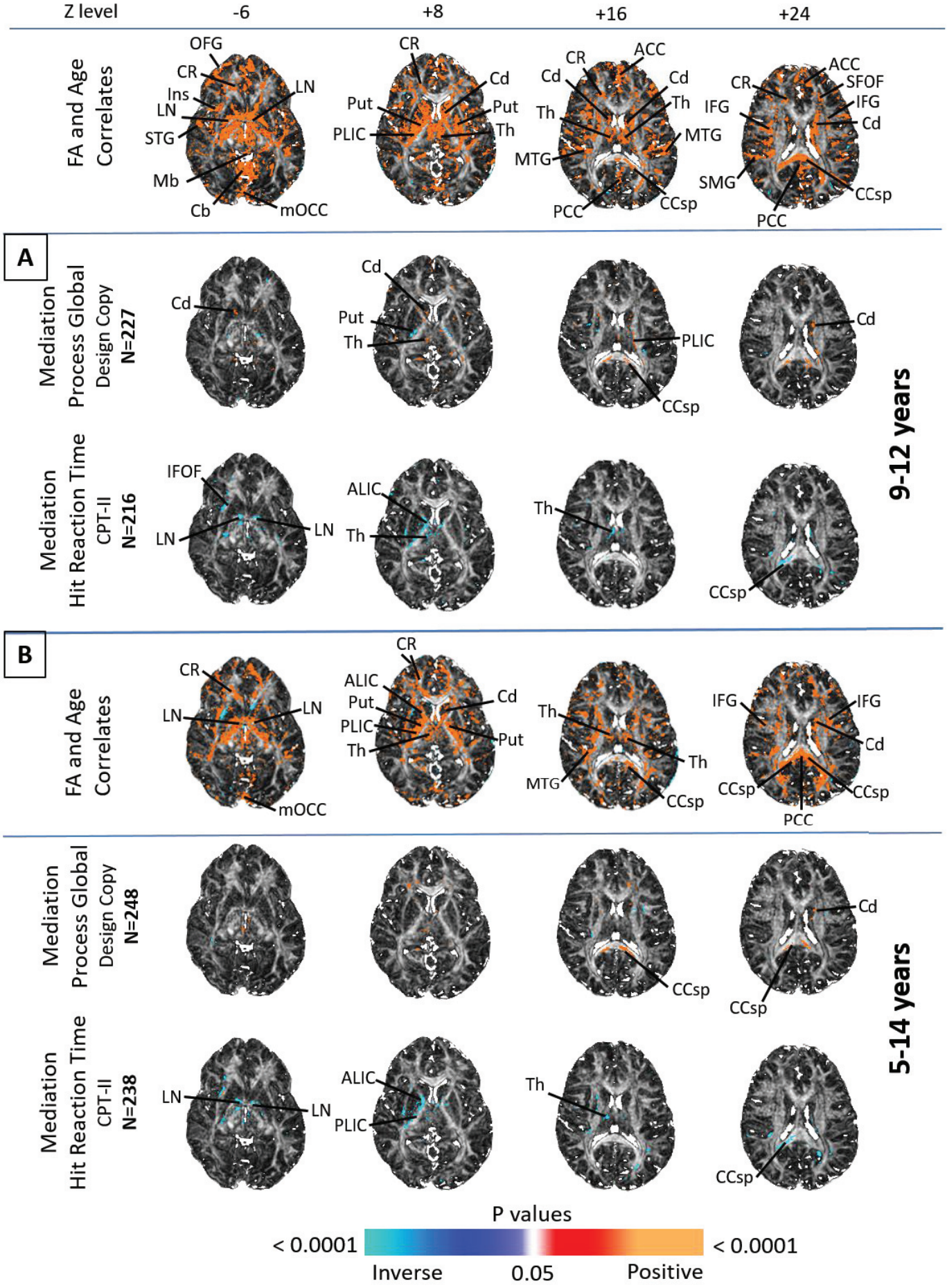

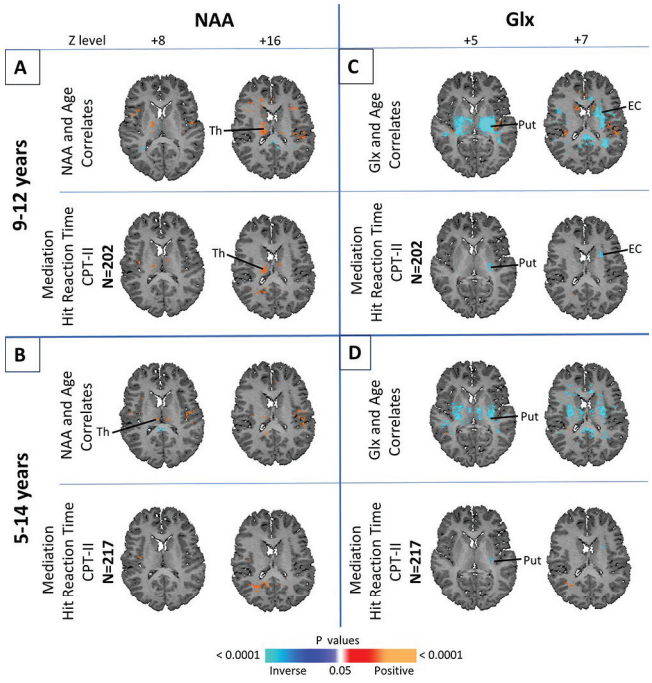

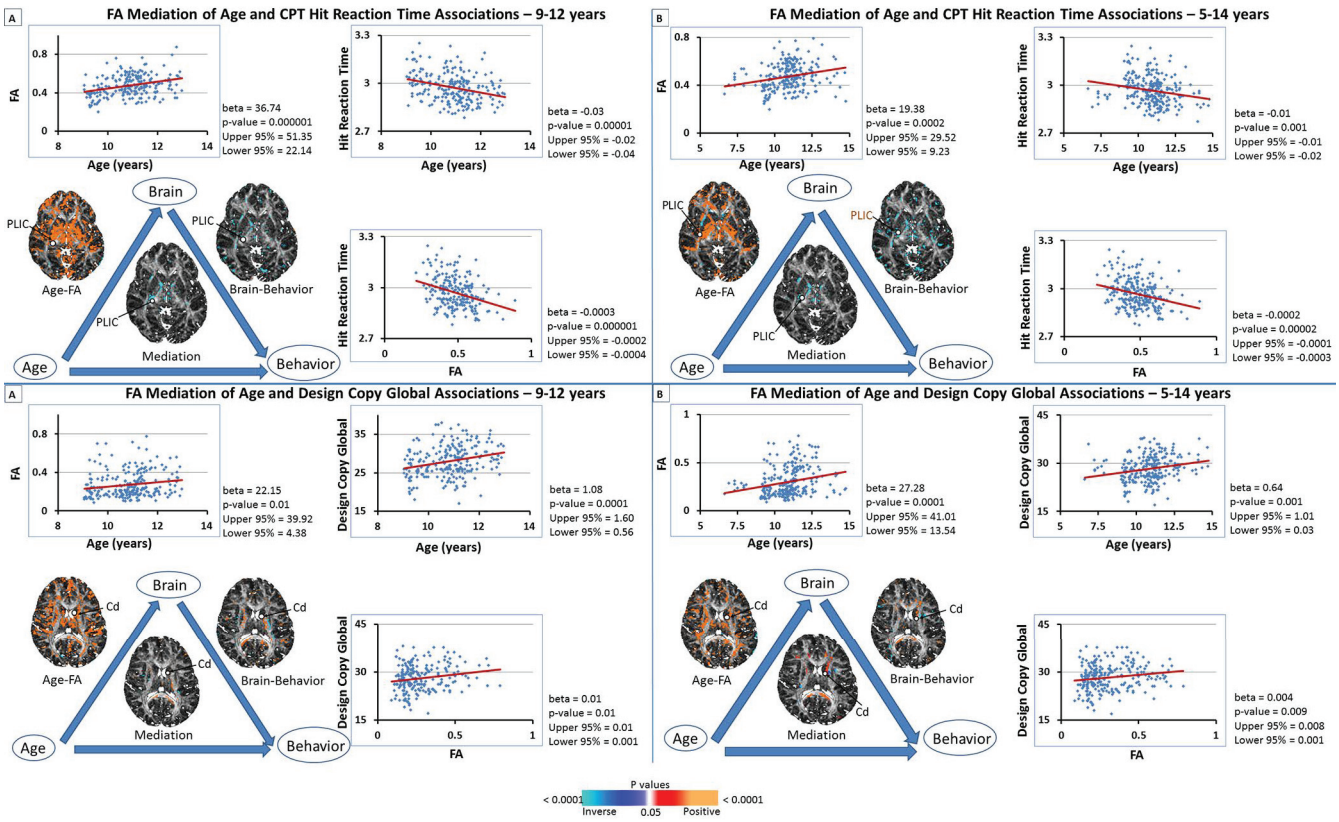

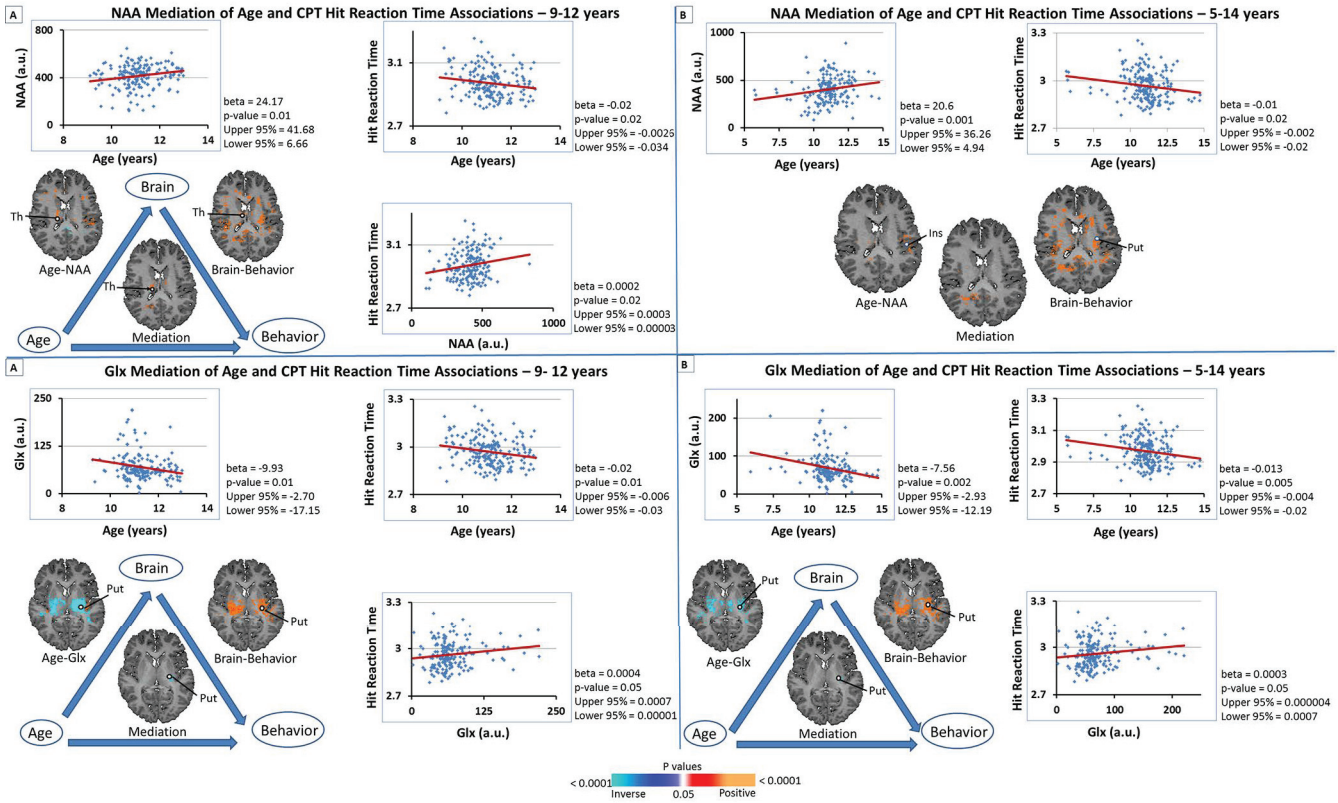

Table 1. Demographics of Study Population

Characteristic	Age 9-12 Years (n=280)	Age 5-14 Years (n=309)
Age (years)	10.86 ± 0.99	10.77 ± 1.40
Gender	Female - 148 (52.9%) Male - 132 (47.1%)	Female – 165 (53.4%) Male – 144 (46.6%)
Race/ethnicity	Dominican/Dominican American – 168 (60%) African American – 112 (40%)	Dominican/Dominican American – 186 (60.2%) African American – 123 (39.8%)
WISC FSIQ	94.8 ± 12.1 (range 69-123)	95.0 ± 12.2 (range 54-129)
Maternal Education (years)	≤ 8th grade – 5 (1.9%) 9th to < 12th grade – 58 (20.7%) High school graduate – 73 (26.1%) 1-4 years of college – 123 (43.8%) 1-4 years of graduate education – 21 (7.5%)	≤ 8th grade – 5 (1.6%) 9th to < 12th grade – 64 (20.7%) High school graduate – 82 (26.5%) 1-4 years of college – 137 (44.3%) 1-4 years of graduate education – 21 (6.9%)
Material Hardship Score[1]	0 – 167 (59.6%) 1 – 59 (21.1%) 2 – 54 (19.3%) 3, 4 - 0	0 – 182 (58.9%) 1 – 66 (21.4%) 2 – 61 (19.7%) 3, 4 - 0

[1] Mothers were asked, “In the past year has there been a time when you: 1. couldn't afford to buy food?; 2. couldn't afford a place to stay?; 3.couldn't afford gas/electricity?; or 4. couldn't afford clothing?” Each positive response to one of the 4 questions was scored with one point.

Table 2. Demographics of Study Population by Imaging Modality

Characteristic	Age 9-12 Years	Range	Age 5-14 Years	Range
Age (years)				
DTI only	10.10 ± 0.95 (n=66)	9.1-12.8	10.14 ± 1.48 (n=73)	5.9-14.1
MRS only	10.92 ± 1.01 (n=46)	9.3-12.9	10.79 ± 1.17 (n=48)	7.3-12.9
DTI & MRS	11.14 ± 0.83 (n=168)	9.1-12.9	11.01 ± 1.35 (n=188)	6.6-14.7
Gender				
DTI only	Female - 35 (53%) Male - 31 (47%)		Female – 40 (54.8%) Male – 33 (45.2%)	
MRS only	Female - 20 (43.5%) Male - 26 (56.5%)		Female – 21 (43.8%) Male – 27 (56.3%)	
DTI & MRS	Female - 93 (55.4%) Male - 75 (56.5%)		Female – 104 (55.3%) Male – 84 (44.7%)	
Race/ethnicity				
DTI only	Dominican/Dominican American – 44 (66.7%) African American – 22 (33.3%)		Dominican/Dominican American – 50 (66.5%) African American – 23 (31.5%)	
MRS only	Dominican/Dominican American – 23 (50%) African American – 23 (50%)		Dominican/Dominican American – 23 (47.9%) African American – 25 (52.1%)	
DTI & MRS	Dominican/Dominican American – 103 (61.3%) African American – 65 (38.7%)		Dominican/Dominican American – 113 (60.1%) African American – 75 (39.9%)	
WISC FSIQ				
DTI only	91.5 ± 11.3	71-117	91.7 ± 11.2	78-109

MRS only	93.6 ± 13.2	54-123	93.1 ± 13.4	71-91
DTI & MRS	96.4 ± 11.8	60-120	96.8 ± 12.0	75-129
Maternal Education (years)				
DTI only	≤ 8th grade – 1 (1.5%) 9th to < 12th grade – 16 (18.2%) High school graduate – 11 (16.7%) 1-4 years of college – 30 (45.5%) 1-4 years of graduate education – 8 (12.1%)		≤ 8th grade – 1 (1.4%) 9th to < 12th grade – 17 (23.3%) High school graduate – 14 (19.1%) 1-4 years of college – 33 (45.2%) 1-4 years of graduate education – 8 (11%)	
MRS only	≤ 8th grade – 0 (0%) 9th to < 12th grade – 11 (23.9%) High school graduate – 12 (26.1%) 1-4 years of college – 19 (41.3%) 1-4 years of graduate education – 4 (8.7%)		≤ 8th grade – 0 (0%) 9th to < 12th grade – 11 (12.5%) High school graduate – 13 (27.1%) 1-4 years of college – 20 (41.7%) 1-4 years of graduate education – 4 (8.3%)	
DTI & MRS	≤ 8th grade – 4 (1.2%) 9th to < 12th grade – 31 (19.6%) High school graduate – 50 (29.8%)		≤ 8th grade – 4 (1.1%) 9th to < 12th grade – 36 (20.2%) High school graduate – 55 (30.3%)	

	1-4 years of college – 64 (44.1%) 1-4 years of graduate education – 9 (5.4%)		1-4 years of college – 84 (44.7%) 1-4 years of graduate education – 9 (4.8%)	
Material Hardship Score[1]				
DTI only	0 – 35 (53%) 1 – 12 (18.2%) 2 – 19 (28.8%) 3, 4 - 0		0 – 36 (49.3%) 1 – 14 (19.2%) 2 – 23 (31.5%) 3, 4 - 0	
MRS only	0 – 26 (56.5%) 1 – 13 (28.3%) 2 – 7 (15.2%) 3, 4 - 0		0 – 28 (58.3%) 1 – 13 (27.1%) 2 – 7 (14.6%) 3, 4 - 0	
DTI & MRS	0 – 106 (63.1%) 1 – 34 (20.2%) 2 – 28 (16.7%) 3, 4 - 0		0 – 118 (62.8%) 1 – 39 (20.7%) 2 – 31 (16.5%) 3, 4 - 0	

[1] Mothers were asked, “In the past year has there been a time when you: 1. couldn't afford to buy food?; 2. couldn't afford a place to stay?; 3.couldn't afford gas/electricity?; or 4. couldn't afford clothing?” Each positive response to one of the 4 questions was scored with one point.

Table 3: Significant Correlations of Neurocognitive Scores* with Age

Instrument	Task	Subscale	Correlation	p-value
NEPSY	INI Inhibition	Total self-corrected errors**	-0.16	0.02
	INS Switching	Total uncorrected errors**	-0.19	0.01
		Total errors**	-0.18	0.01
	Auditory Attention	Total commission errors**	-0.23	0.001
		Total omission errors**	-0.21	0.002
	Response Set	Total commission errors**	-0.30	0.0003
		Total omission errors**	-0.19	0.006
		Total inhibitory errors**	-0.26	0.001
	Naming	Uncorrected errors**	-0.19	0.004
		Total errors	-0.15	0.03
	Design Copy	Process total	0.29	<0.0001
		Process local	0.28	0.00002
		Process global	0.23	0.0005
		Process motor	0.24	0.0002
		Global total	0.21	0.002
Conners' CPT	Total Overall	Omission errors	-0.13	0.05
		Commission errors**	-0.17	0.01
		Hit reaction time**	-0.24	0.0004
		Detectability d'	0.18	0.01

*All were raw scores, unadjusted for participant age or sex

**when transformed, those raw scores also correlated with age